



HAL
open science

Preparation of chains of magnetosomes, isolated from AMB-1 magnetotactic bacteria, yielding efficient treatment of tumors using magnetic hyperthermia

Edouard Alphandéry, François Guyot, Imène Chebbi

► **To cite this version:**

Edouard Alphandéry, François Guyot, Imène Chebbi. Preparation of chains of magnetosomes, isolated from AMB-1 magnetotactic bacteria, yielding efficient treatment of tumors using magnetic hyperthermia. International Journal of Pharmaceutics, 2012, 434 (1-2), pp.444 - 452. 10.1016/j.ijpharm.2012.06.015 . hal-01547081

HAL Id: hal-01547081

<https://hal.sorbonne-universite.fr/hal-01547081v1>

Submitted on 26 Jun 2017

HAL is a multi-disciplinary open access archive for the deposit and dissemination of scientific research documents, whether they are published or not. The documents may come from teaching and research institutions in France or abroad, or from public or private research centers.

L'archive ouverte pluridisciplinaire **HAL**, est destinée au dépôt et à la diffusion de documents scientifiques de niveau recherche, publiés ou non, émanant des établissements d'enseignement et de recherche français ou étrangers, des laboratoires publics ou privés.

1 Preparation of chains of magnetosomes, isolated from
2 AMB-1 magnetotactic bacteria, yielding efficient
3 treatment of tumors using magnetic hyperthermia

4 *Edouard Alphandéry^{+,‡,*}, François Guyot^{+,x}, Imène Chebbi[‡],*

5 ⁺Institut de minéralogie et de physique des milieux condensés, Université Pierre et Marie Curie, UMR
6 CNRS 7590, 4 Place Jussieu, 75005, Paris.

7 [‡]Nanobacterie SARL, 36 boulevard Flandrin, 75016, Paris.

8 ^xUniversité Paris Diderot, Sorbonne Paris Cité, Institut de Physique du Globe de Paris, 1 Rue Jussieu,
9 75005, Paris

10 *CORRESPONDING AUTHOR CONTACT DETAILS:

11 E-MAIL edouardalphandery@hotmail.com

12 Phone: 33632697020.

13 Adresse: Nanobacterie, 36 boulevard Flandrin, 75016, Paris, France.

14 No fax.

15

16

17 **ABSTRACT**

18 Chains of magnetosomes isolated from AMB-1 magnetotactic bacteria by sonication at 30 W during 2
19 hours are tested for magnetic hyperthermia treatment of tumors. These chains are composed of
20 magnetosomes, which are bound to each other by a filament made of proteins. When they are incubated
21 in the presence of cancer cells and exposed to an alternating magnetic field of frequency 198 kHz and
22 average magnetic field strength of 20 or 30 mT, they produce efficient inhibition of cancer cell
23 proliferation. This behavior is explained by a high cellular internalization, a good stability in solution
24 and a homogenous distribution of the magnetosome chains, which enables efficient heating. When the
25 chains are heated during 5 hours at 90 °C in the presence of 1 % SDS, the filament binding the
26 magnetosomes together is denatured and individual magnetosomes are obtained. By contrast to the
27 chains of magnetosomes, the individual magnetosomes are prone to aggregation, are not stable in
28 solution and do not produce efficient inhibition of cancer cell proliferation under application of an
29 alternating magnetic field.

30

31

32

33

34

35

36 **KEYWORDS**

37 Magnetosomes, magnetotactic bacteria, cancer, tumor, chains of magnetosomes, individual
38 magnetomes, alternating magnetic field, magnetic hyperthermia.

39 1. INTRODUCTION

40 Magnetic hyperthermia is a technique by which magnetic nanoparticles are either introduced or sent
41 within tumors and heated under the application of an alternating magnetic field (AMF). The heat
42 produced locally by the nanoparticles induces anti-tumoral activity. Magnetic hyperthermia has been
43 used both on animal models and on humans to treat a series of different cancers, including breast cancer,
44 [1, 2], prostate cancer, [3-6], glioblastoma, [7], and head and neck cancer, [8]. Until now, most of the
45 iron oxide nanoparticles tested were chemically synthesized with either a superparamagnetic or a weakly
46 ferrimagnetic behavior at physiological temperature, [9-12]. For an applied magnetic field of frequency
47 and strength kept below a toxicity threshold of ~ 200 kHz and ~ 100 mT respectively, [13], the specific
48 absorption rate (SAR) of the chemically synthesized nanoparticles is lower by a factor of 2 to 100 than
49 that of the biologically synthesized nanoparticles, called magnetosomes, [9-11]. For this reason, there
50 has been a surge of interest to carry out magnetic hyperthermia for cancer treatment using the
51 magnetosomes, [14-18]. In fact, the magnetosomes are monodomain, well-crystallized nanoparticles
52 surrounded by a lipidic membrane with the unique property of being usually arranged in chains. They
53 are synthesized by a species of bacteria, called magnetotactic bacteria, which use them as a compass to
54 navigate in the direction of the earth magnetic field in search for an optimum environment. In a previous
55 study, [18], 1 mg of a suspension of chains of magnetosomes extracted from AMB-1 magnetotactic
56 bacteria has been administered within breast tumors xeno-grafted under the skin of mice. After three
57 applications of an alternating magnetic field during 20 minutes, tumors were totally eradicated in several
58 mice. These results suggest that chains of magnetosomes extracted from AMB-1 magnetotactic bacteria
59 are highly efficient for solid tumor treatment using magnetic hyperthermia, [18].

60 In this article, we examine if the efficiency of chains of magnetosomes extracted from AMB-1
61 magnetotactic bacteria, designated as CM, is solely due to the high SAR of the magnetosomes or if it
62 also arises from other factors such as a homogenous distribution of the magnetosome chains within the
63 tissue or a faculty of the magnetosome chains to internalize within the cancer cells. To know the

64 influence of the magnetosome chain arrangement on the efficiency of the therapy, we compare the
65 properties of the chains of magnetosomes with those of individual magnetosomes, designated as IM,
66 which are detached from the chains by heat and chemical treatments.

67 2. MATERIALS AND METHODS

68 2.1 Method used for the culture of the AMB-1 magnetotactic bacteria:

69 Magnetotactic bacteria belonging to the species *Magnetospirillum magneticum*, strain AMB-1, available
70 at the ATCC under the reference 700264, were cultivated in a volume of 1 liter of bacterial growth
71 medium. The cells were cultivated in micro-anaerobic conditions, *i. e.* in a culture medium that has not
72 been degassed, but is closed and not in contact with oxygen. The culture of magnetotactic bacteria has
73 been carried out in an incubator at 26 °C in a slightly modified MSGM liquid culture medium, whose
74 composition is described below.

75 For a volume of 1 liter, the standard culture medium contains 0.68 g of monobasic potassium phosphate,
76 0.85 g of sodium succinate, 0.57 g of sodium tartrate, 0.083 g of sodium acetate, 225 µl of 0.2 %
77 resazurine, 0.17 g of sodium nitrate, 0.04 g of L-ascorbic acid, 2 ml of a 10 mM solution of iron quinate,
78 10 mL of a solution of Woolf's vitamins and 5 mL of a solution of Woolf's minerals. The solution of
79 iron quinate has been prepared by dissolving 0.19 g of quinic acid and 0.29 g of FeCl₃.6H₂O in 100 ml
80 of distilled water. The solution of Woolf's minerals contains in 1 liter of distilled water, 0.5 g of
81 nitrilotriacetic acid (NTA, C₆H₉O₆), 1.5 g of magnesium sulfate heptahydrate (MgSO₄.7H₂O), 1 g of
82 sodium chloride, 0.5 g of manganese sulfate monohydrate (MnSO₄.H₂O), 100 mg of iron sulfate
83 heptahydrate (FeSO₄.7H₂O), 100 mg of cobalt nitrate heptahydrate (Co(NO₃)₂.7H₂O), 100 mg of
84 calcium chloride (CaCl₂), 100 mg of zinc sulfate heptahydrate (ZnSO₄.7H₂O), 10 mg of copper sulfate
85 pentahydrate (CuSO₄.5H₂O), 10 mg of aluminium potassium sulfate, 10 mg of potassium dodecahydrate
86 (AlK(SO₄).12H₂O), 10 mg of boric acid (H₃BO₃), 10 mg of sodium molybdate dehydrate
87 (Na₂MoO₄.2H₂O), 2 mg of sodium selenite (Na₂SeO₃), 10 mg of sodium tungstate dihydrate

88 (Na₂WO₄·2H₂O) and 20 mg of nickel chloride hexahydrate (NiCl₂·6H₂O). The solution of Woolf's
89 vitamins was prepared by dissolving in one liter of distilled water, 2.2 mg of folic acid (vitamin B9),
90 10.2 mg of pyridoxine (vitamin B6), 5.2 mg of riboflavin (vitamin B2), 5.2 mg of pantothenic acid
91 (vitamin B5), 0.4 mg of vitamin B12, 5.2 mg of amino-benzoic acid, 5.2 mg of thiotic acid and 900 mg
92 of potassium phosphate. The pH of the culture medium was adjusted to 6.85 by using a 1 M solution of
93 sodium hydroxide.

94 *2.2 Preparation of the different suspensions containing the extracted chains of magnetosomes and*
95 *individual magnetosomes:*

96 Two different types of magnetosomes have been isolated from AMB-1 magnetotactic bacteria, those
97 arranged in chains and those forming individual nanoparticles. To prepare them, the cells were first
98 harvested by centrifugation at 4 000 g during 20 minutes. The supernate was then removed and the cells
99 were re-suspended in deionized water. To extract the chains of magnetosomes, 1 ml of cell suspension
100 obtained as previously described was centrifugated again and re-suspended in a 10 ml tris-HCl buffer of
101 pH 7.4. The cellular suspension was then sonicated during 120 minutes at 30 W in order to lyse the cells
102 and collect the CM. After sonication, the suspension containing the CM was separated from the cellular
103 debris by positioning a strong neodymium magnet (0.1-1 T) next to the tube, and the magnetic material
104 was then harvested. The supernate containing the cellular debris and other organic molecules was
105 eliminated. CM were washed 10 to 20 times in deionized water at pH 7.4 and were then resuspended in
106 deionized water. To prepare the suspensions containing the IM, the suspension containing the CM was
107 heated during five hours at 90 °C in the presence of 1 % SDS. IM were separated from the biological
108 material remaining after the treatment by using a strong neodymium magnet (0.1-1T). The concentrations
109 in maghemite of the various suspensions containing CM and IM were measured by absorption at 480
110 nm, [18].

111 *2.3 Methods used for measuring the SAR and for heating the different suspensions of bacterial*
112 *magnetosomes:*

113 The SAR of suspensions of CM and IM were measured for bacterial magnetosomes, which were either
114 able or unable to rotate under the application of an AMF, [16]. The amount of heat produced in the gel
115 by the CM and IM was low under the application of an AMF of frequency 108 kHz and magnetic field
116 strength kept below 36 mT, [16]. To enhance the magnetosome heating efficiency during the *in-vitro*
117 and *in-vivo* heating experiments, the frequency of the AMF was therefore increased up to 198 kHz and
118 the average magnetic field strength was kept below 30 mT to avoid the formation of eddy currents,
119 which can induce toxicity. The average magnetic field strength was estimated from the variation with
120 time of the magnetic field strength. It was measured using a 2D magnetic field probe designed by the
121 company Fluxtrol. The value of the average magnetic field strength measured experimentally with this
122 probe was 1.8 times lower than the theoretical value of the magnetic field, estimated using the relation B
123 $= \mu_0 NI/L$, where $\mu_0 = 4\pi 10^{-7}$ is the vacuum permeability, $N = 4$ is the number of spires in the coil, $I =$
124 151, 300, 419 or 600 A is the amplitude of the alternating current flowing through the spires and $L = 3.5$
125 cm is the length of the coil (Suppl. table 1). The temperatures reached during the heating experiments
126 were measured using a thermocouple microprobe (IT-18, Physitemp, Clifton, USA).

127 *2.4 Percentage of inhibition and magnetization studies of HeLa and MDA-MB 231 cells incubated in the*
128 *presence of the different suspensions of magnetosomes isolated from AMB-1 magnetotactic bacteria:*

129 The HeLa and MDA-MB 231 cells were purchased from the ATCC. The cell lines were cultivated in
130 Dulbecco's model modified Eagle's medium supplement, which contained 10% fetal calf serum, 2 mM
131 L-glutamine, 1 mM sodium pyruvate, and 50 U/mL streptomycin (all purchased from Life Technologies
132 Inc.). Cell viability was evaluated using the so-called MTT (microculture tetrazolium) assay, [19]. This
133 technique measures the ability of mitochondrial enzyme to reduce 3-(4,5-dimethylthiazol-2-yl)-2,5-
134 diphenyltetrazolium bromide (purchased from Sigma, St Louis, MO, USA) to purple formazan crystals.
135 MDA-MB-231 and HeLa cells were seeded at a density of $2 \cdot 10^4$ cells per well in 96-well flat-bottom
136 plates (Falcon, Strasbourg, France) and incubated in completed culture medium for 24 hours. Then, the
137 culture medium was removed and replaced by 10 % FCS-medium containing CM or IM with different

138 concentrations in iron oxide (1 mg/mL, 500 µg/mL or 125 µg/mL). After 24 hours of incubation, the
139 cells were exposed (or not) to an AMF of frequency 198 kHz and average magnetic field strength of ~
140 20 mT or ~ 30 mT during 20 min. After having been exposed to the AMF, the cells were incubated at 37
141 °C in a 5 % CO₂ humidified atmosphere during 48 hours. Following the incubation, cells were washed
142 with phosphate buffered saline solution (PBS, Life Technologies) and incubated with 100 µl of MTT (2
143 mg/ml, Sigma-Aldrich) for an additional 4 hours at 37 °C. The insoluble product was then dissolved by
144 addition of 100 µl of DMSO (Sigma-Aldrich). The absorbance of the solubilized formazan pellet,
145 which reflects the relative viable cell number, was measured at 540 nm using a Labsystems Multiskan
146 MS microplate reader. The measurements were carried out on DMSO solubilized formazan pellets using
147 cells washed with PBS as a control, [20]. The experiments were carried out in triplicates.

148 *2.5 Internalization and magnetization studies of MDA-MB 231 cells incubated in the presence of*
149 *various suspensions of magnetosomes:*

150 5.10⁵ MDA-MB-231 cells in suspension were mixed in 1 ml of a 10 % FCS-medium containing
151 suspensions of CM or IM with a fixed concentration in iron oxide of 1 mg/ml. The cells were exposed
152 (or not) to an AMF of frequency 198 kHz and average field strength of ~ 20 mT during 5, 10, 15 and 20
153 minutes. Following the application of the AMF, the MDA-MB-231 cells were collected with a strong
154 neodymium magnet (0.1-1 T). For each sample, 10⁴ cells were used to quantify the mass of iron oxide
155 per cell. Solutions containing various concentrations of FeCl₃ mixed with potassium thiocyanate (2 M)
156 were prepared for calibration. Solutions containing one volume of HCl (6 N) mixed with 20 volumes of
157 H₂O₂ were added to the cells to dissolve the iron oxide into Fe³⁺ ions and to denature all biological
158 material. The cells were further lysed by sonication during 30 minutes at 30 W (0 °C) and mixed with a
159 solution of potassium thiocyanate (2 M), which induces the formation of a complex composed of Fe³⁺
160 and SCN⁻. Quantification of iron oxide was estimated by absorption measurements at 480 nm (UVICON
161 923, Bio-Tek, Kontron Instrument, Italy). The untreated MDAMB-231 cells were used as reference. The
162 experiments were carried out in triplicates.

163 *2.6 In vitro Prussian blue assay:*

164 MDA-MB-231 cells were seeded on Petri dishes (\varnothing 30 mm, density $\sim 5 \cdot 10^5$ cells per Petri dish), grown
165 during 24 hours and incubated (or not) during 24 hours in the presence of suspensions of CM or IM at a
166 concentration of 142 $\mu\text{g}/\text{mL}$. Cells were washed twice in PBS and fixed in 4 % paraformaldehyde (PFA)
167 (Sigma) during 15 minutes at 4 °C. MDA-MB-231 cells were washed twice more time in PBS and were
168 then stained with Perl's Prussian blue solution during 20 minutes at 37 °C in an atmosphere containing 5
169 % CO_2 . Perl's Prussian blue solution was prepared by mixing two solutions of equal volumes containing
170 4 % potassium ferrocyanide and 4 % HCl. Staining (bright blue pigment: $\text{Fe}^{\text{III}}[\text{Fe}^{\text{III}}\text{Fe}^{\text{II}}(\text{CN})_6]_3$) resulted
171 from the reaction between Fe^{2+} or Fe^{3+} ions coming from the dissolved magnetosomes and the
172 ferrocyanide ions. After having washed each Petri dish three times with PBS, Prussian blue staining was
173 observed using an optical microscope. The experiments were carried out in triplicates.

174 *2.7 Scanning electron microscopy, transmission electron microscopy and optical microscopy studies of*
175 *MDA-MB 231 cells incubated in the presence of either chains of magnetosomes or individual*
176 *magnetosomes:*

177 Scanning electron microscopy (SEM) studies were carried out using a FEG-SEM ultra 55 from Zeiss
178 equipped with an energy dispersive X-ray analysis system (EDX). The samples studied by SEM
179 contained MDA-MB-231 cancer cells incubated during 24 hours in the presence of IM or CM. The cells
180 were deposited on top of a carbon grid covered with a carbon film and fixed with NOVAprep, produced
181 by Novacyt. Transmission electron microscopy (TEM) studies were also carried out using a JEOL
182 2100F-FEG operated at 200 kV. The samples studied by TEM contained 5 μl of suspensions of IM or
183 CM deposited on top of a carbon grid. Optical microscopy was also used to visualize precipitated
184 magnetosomes within MDA-MB 231 cells. For that, the cells were incubated in the presence (or not) of
185 suspensions containing either CM or IM. The cells were stained with Prussian blue, which precipitates
186 in the presence of iron, producing a blue color in the micrographs, which reveals the presence of iron.

188 3.1 The different types of bacterial magnetosomes chosen for magnetic hyperthermia treatment of
189 tumors:

190 In whole magnetotactic bacteria, the chains of magnetosomes only occupy a small portion of the total
191 volume of a bacterium ($\sim 0.02\%$). A TEM image of a typical AMB-1 magnetotactic bacterium is shown
192 in Figure 1(a). Several chains of magnetosomes separated by more than ~ 100 nm are contained within
193 this bacterium. Large regions of the bacterium are not occupied by chains of magnetosomes. Because of
194 the low density of the chains of magnetosomes within whole magnetotactic bacteria, suspensions
195 containing whole magnetotactic bacteria are expected to yield a low *in vivo* heating efficiency. In
196 addition, the administration of whole inactive magnetotactic bacteria in humans is not recommended due
197 to the presence of potentially toxic biologic materials such as bacterial DNA or endotoxins, [21]. For
198 these two reasons, whole inactive magnetotactic bacteria were not tested in this study. In order to
199 minimize the risks of toxicity and to enhance the heating efficiency, the bacterial magnetosomes were
200 isolated from the bacteria.

201 The first type of bacterial magnetosomes tested for magnetic hyperthermia consisted of chains of
202 magnetosomes extracted from AMB-1 magnetotactic bacteria, CM. Figure 1(b) shows a TEM image of
203 a suspension of CM deposited on top of a carbon grid. The extraction of the chains of magnetosomes
204 from the bacteria yields an increase in the concentration of the chains of magnetosomes (Figures 1(a)
205 and 1(b)). The magnetosome chains also appear to be longer than in whole bacteria. When chains of
206 magnetosomes are extracted from the magnetotactic bacteria, they interact with each other in such a way
207 that they form longer chains. This type of interaction yields a homogeneous distribution of CM within
208 the substrate (Figure 1(b)). To assess the stability of CM mixed in water, their zeta potential was
209 measured as a function of pH by dynamic laser light scattering (DLS) on a Nano-ZS (Red Badge) ZEN
210 3600 device (Malvern Instruments, Malvern, UK). For a suspension of CM, which is homogenized by
211 sonication, Figure 2(a) shows that the variations of the zeta potential as a function of pH is very similar

212 to that obtained for a non sonicated suspension of CM. This indicates the good stability of the
213 suspension of CM mixed in water. To examine if CM have kept the biological material surrounding
214 them after extraction, infra-red absorption measurements were carried out on CM. Figure 2(b) depicts
215 the infra-red absorption spectrum of a powder containing a lyophilized suspension of chains of
216 magnetosomes denatured and solubilized with KBr. It shows two absorption peaks at 1650 cm^{-1} (peak 1,
217 Figure 2(b)) and 1530 cm^{-1} (peak 2, Figure 2(b)), which arise from the Amide I and Amide II bands and
218 are due to the absorption of proteins, [21-23]. The peaks at 1250 cm^{-1} (peak 3, Figure 2(b)) and 1050
219 cm^{-1} (peak 4, Figure 2(b)) can either be attributed to the absorption of lipopolysaccharide (LPS) or
220 phospholipids [23,24], both located within the magnetosome membrane, [20]. The peak at 580 cm^{-1}
221 (peak 5, Figure 2(b)) is attributed to maghemite, [25]. These results suggest that both the filament
222 binding the magnetosomes together, which is made of proteins such as MamJ or Mam K, [26-28], and
223 the bilayer surrounding the individual magnetosomes, which is composed of LPS and phospholipids,
224 [29], are contained within CM. After extraction, the magnetosome chains have kept the lipid bi-layer
225 surrounding each magnetosome and the filament binding the magnetosomes together.

226 To obtain suspensions of magnetosomes, which are similar to the chemically synthesized iron oxide
227 nanoparticles, *i. e.* not arranged in chains, IM have been prepared by heating a suspension of CM at 90
228 $^{\circ}\text{C}$ during 5 hours in the presence of 1 % SDS. TEM images of a suspension of IM deposited on top of a
229 carbon grid are presented in Figures 1(c) and 1(d). It shows either assemblies of magnetosomes, which
230 are much more aggregated than the chains of magnetosomes (Figure 1(c)), or loops (Figure 1(d)). At pH
231 = 7, Figure 2(a) shows that suspensions of IM possess very different values of their zeta potential
232 depending on whether or not they are mixed homogeneously by sonication. When IM are mixed
233 homogeneously in solution, they possess a negative zeta potential of $\sim -35\text{ mV}$ at pH ~ 7 , [30]. When
234 they are not sonicated, the IM zeta potential is 10 mV at pH ~ 7 . The different values of the Zeta
235 potential suggest that IM easily form aggregates in solution and are therefore unstable in the absence of
236 sonication, [30]. The infra-red absorption spectrum of a powder containing a lyophilized suspension of

237 IM integrated in a KBr matrix is presented in Figure 2(b). It shows Amide I and Amide II peaks (peaks 1
238 and 2, Figure 2(b)), suggesting that most of the proteins contained in the filament binding the
239 magnetosomes together have been removed. The relatively strong peaks at 1050 cm^{-1} and 1240 cm^{-1}
240 suggest that the bi-layer surrounding each magnetosome has not been significantly removed during the
241 heat treatment in the presence of a detergent.

242 *3.2 SAR of the different suspensions of bacterial magnetosomes:*

243 The SAR of suspensions containing IM and CM were measured in two situations in which the bacterial
244 magnetosomes were either able or unable to rotate under the application of an AMF, [16]. For the
245 bacterial magnetosomes mixed in water and able to rotate, Figures 3(a) and 3(b) show that the amount of
246 heat produced by the CM is larger than that produced by the IM. This behavior could be explained by
247 the fact that CM are less prone to aggregation and therefore rotate more easily than IM under the
248 application of an AMF. This analysis is further supported by the TEM image presented in Figure 1(b),
249 which clearly shows that CM do not aggregate by contrast to IM (Figure 1(c)). For the bacterial
250 magnetosomes mixed in water, the higher value of the SAR obtained for CM compared with IM could
251 therefore be explained by a contribution of the rotation to the heat production, which is more significant
252 for CM than for IM. By contrast, when CM and IM are fixed (either in a gel or on a solid substrate,
253 [16]), unable to rotate, mixed homogeneously and exposed to the same AMF as above, IM produce a
254 relatively similar amount of heat than CM (Figure 3), [16]. These results suggest that when the rotation
255 of the magnetosomes is not taking part in the mechanism of heat production, which is most probably the
256 case *in vivo*, the quantity of heat generated by CM or IM is not only due to the magnetosome SAR but
257 also to the spatial distribution of the magnetosomes.

258 *3.3 Percentage of inhibition of HeLa and MDA-MB-231 cells incubated in the presence of CM or IM:*

259 To compare the anti-tumoral activity of CM with that of IM, CM and IM were incubated in the presence
260 of HeLa and MDA-MB-231 cells. The percentage of inhibition of cellular proliferation was then

261 measured in the presence (or not) of an AMF. The results are presented for two suspensions of bacterial
262 magnetosomes (CM or IM) with a concentration fixed at 0.125 mg/ml. In the absence of application of
263 an AMF, the percentages of inhibition of MDA-MB-231 and HeLa cells incubated in the presence of
264 CM or IM were as low as 2 % and 10 % (Figure 4(a)), respectively. When these cancer cells were
265 incubated in the presence of the CM and exposed to an AMF of frequency 198 kHz and average
266 magnetic field strength of 20 mT and 30 mT, the percentages of inhibition increased by factors of ~ 3 to
267 ~ 5 for the HeLa cells and ~ 7 to ~ 16 for the MDA-MB-231 cells (Figure 4(a)). By contrast, when these
268 cancer cells were incubated in the presence of IM and exposed to the same AMF as above, the
269 percentage of inhibition of these cells remained almost identical (Figure 4(a)). A similar type of
270 behavior was observed when MDA-MB6231 and HeLa cells were incubated in the presence of CM and
271 IM at higher iron oxide concentrations of 1 mg/ml (Suppl. Fig. 1(a)) and 0.5 mg/ml (Suppl. Fig. 1(b)).
272 These results indicate that under the application of an AMF, CM yield a higher percentage of cell
273 inhibition than IM.

274 *3.4 Penetration of the chains of magnetosomes within the cancer cells under the application (or not) of* 275 *an alternating magnetic field:*

276 We examine if the different efficiencies observed between CM and IM are due to a different faculty of
277 penetration within the cancer cells of these two types of bacterial magnetosomes. We first study if the
278 application of an AMF induces the internalization of CM or IM within the cancer cells. To be able to
279 estimate the magnetization of MDA-MB-231 cells, the latter had to be kept free and not fixed. The cells
280 were incubated in the presence of the CM and IM and exposed to the same AMF as above. The cancer
281 cells were then washed with water to remove CM and IM located at their surface and the percentage of
282 magnetic cells was then measured. Following application of an AMF of frequency 198 kHz during 5 to
283 20 minutes, Figure 4(b) shows that the mass of maghemite per magnetic cell is always much higher for
284 the cells incubated in the presence of CM than for those incubated in the presence of IM. This result
285 suggests that under the application of an AMF, CM penetrate much more within the cancer cells than

286 IM. Moreover, the high cellular magnetization, which can be reached in the presence of CM under the
287 application of an AMF, could explain the high efficiency of CM for magnetic hyperthermia treatment of
288 tumors.

289 We also study the internalization of CM and IM within the cancer cells as a function of the incubation
290 time in the absence of an AMF. For that, the cells had to be fixed on top of a solid substrate. For a very
291 short incubation time of less than 30 seconds, Figure 4(b) shows that neither CM nor IM penetrate
292 within MDA-MB-231 cells. Suspensions containing CM and IM were then incubated in the presence of
293 MDA-MB-231 cells for a longer incubation time of 24 hours. The cells were deposited on top of a
294 carbon grid substrate and imaged under scanning electron microscopy. Figure 5(a) shows a portion of a
295 typical MDA-MB-231 cell. Enlargements of two regions of the cell in which CM are observed are
296 presented in Figures 5(b) and 5(c). Since CM are observed within intracellular vesicles, designated as V
297 in Figure 5(b), which can be lysosomes or endosomes, CM are internalized within the cancer cell. The
298 chain of magnetosome surrounded by a green box in Figures 5(c) and 5(d) contains two large
299 magnetosomes at its end and several small magnetosomes at the middle. This type of magnetosome
300 arrangement is clearly different from that observed for the magnetosome chains, which are not incubated
301 in the presence of cancer cells (Figure 1(b)). It could be due to the degradation of the chains of
302 magnetosomes by the cells following their internalization. Another reason why CM are internalized
303 within the cells and not bound at the cell surface comes from the fact that the cells were washed prior to
304 the observation by scanning electron microscopy. The presence of CM within the cells was further
305 confirmed by EDX measurements, which revealed the presence of iron oxide in the region where CM
306 were detected (Suppl. Fig. 3). By contrast to the behavior observed with CM, IM were not observed
307 within the MDA-MB-231 cell (Suppl. Fig. 2). The EDX measurements confirmed this behavior (Suppl.
308 Fig. 3). They showed that iron was not detected in the cellular regions with presumably no
309 magnetosomes.

310 The internalization of CM within the cancer cells for a sufficiently long incubation time of 24 hours was
311 further confirmed by optical microscopy. Figure 8 shows optical microscopy observations of MDA-MB-
312 231 cells incubated in the absence of magnetosomes (Figure 8(a)), in the presence of CM during 24
313 hours (Figure 8(b)) or in the presence of IM during 24 hours (Figure 8(c)). For MDA-MB-231 cells
314 incubated in the absence of magnetosomes or in the presence of IM, no Prussian blue coloration was
315 observed within the cells. By contrast, for the MDA-MB-231 cells incubated in the presence of the CM,
316 Prussian blue coloration was observed within the cells. These results agree with those presented above
317 (Figures 5) and suggest that CM penetrate within the cells by contrast to IM, which remain located
318 outside of the cells.

319 *3.5 Explanation for the high efficiency of the chains of magnetosomes:*

320 Altogether, these results indicate that CM penetrate more easily within the cancer cells than IM. While
321 the internalization within the cancer cells did not occur with IM, it was observed for CM in two
322 conditions, either when an AMF of 198 kHz and average field strength of 20 mT was applied during 5 to
323 20 minutes and/or when the cells were incubated with CM for a sufficiently long time of 24 hours. The
324 internalization of CM within the cancer cells could occur by a mechanism of endocytosis or by effective
325 diffusion through the cell membrane. The mechanism of effective diffusion through the cell membrane
326 could be favored by a temperature increase taking place during the application of the AMF, which would
327 make the cell membrane permeable. This result agrees with previous studies, which showed that
328 negatively charged maghemite nanoparticles penetrate within cancer cells, [31]. Since intra-cellular
329 heating presumably efficiently damages cellular components, it may be a more efficient mechanism of
330 cell destruction than extra-cellular heating. The higher efficiency of CM compared with that of IM could
331 therefore be explained by the fact that CM internalize within the cancer cells by contrast to IM, which
332 mostly remain located outside of the cells. Poorly efficient internalization of IM may be related to the
333 more aggregated state of IM compared with that of CM as was observed in two cases, *i. e.* when
334 suspensions of CM and IM were deposited on top of a carbon grid (Figures 1(b) and 1(c)) and *in vivo*

335 when suspensions of CM and IM were administered within tumors xeno-grafted under the skin of mice
336 and heated under the application of an AMF, [18]. A schematic summary showing the different
337 distributions of CM and IM in the presence of cancer cells is proposed in Figures 9(a) and 9(b). The
338 better internalization and more homogenous distribution of CM than IM could provide a reasonable
339 explanation for the higher anti-tumoral efficiency observed for CM than for IM, [18].

340 **4 Conclusion**

341 In conclusion, we have studied two types of bacterial magnetosomes extracted from AMB-1
342 magnetotactic bacteria, the magnetosomes organized in chains and those forming individual
343 magnetosomes detached from the chains by heat and chemical treatment. We have shown that chains of
344 magnetosomes were more efficient than individual magnetosomes in inhibiting cancer cell proliferation
345 under application of an alternating magnetic field. We have suggested that this increased efficiency was
346 related to much less particle aggregation for the magnetosome chains than for the individual
347 magnetosomes and as a consequence to a better faculty for the chains of magnetosomes than for the
348 individual magnetosomes to internalize within the cancer cells. This paper clearly highlights the
349 importance of nanoparticle distribution for efficient magnetic hyperthermia. It shows that the use of
350 nanoparticles with high SAR is not sufficient to yield efficient magnetic hyperthermia.

351 **ACKNOWLEDGMENTS**

352 François Guyot does not claim any inventive contribution in this work. We thank the company
353 NOVAcyt for giving us the NOVAprep product free of charge.

354

355

356

357

358 **Figures:**

359 Figure 1: (a) Transmission electron microscopy image of a typical whole inactive magnetotactic
360 bacterium deposited on top of a carbon grid. The magnetosomes are designated by blue arrows. (b)
361 Transmission electron microscopy image of suspensions of chains of magnetosomes, isolated from
362 magnetotactic bacteria, and deposited on top of a carbon coated copper grid. (c) Transmission electron
363 microscopy images of individual magnetosomes detached from the chains by heat and SDS treatment
364 showing a typical aggregate. (d) Transmission electron microscopy images of individual magnetosomes
365 detached from the chains by heat and SDS treatment showing a loop.

366 Figure 2: (a) Zeta potential of suspensions of chains of magnetosomes and individual magnetosomes as
367 a function of pH. The measurements were carried out with suspensions containing bacterial
368 magnetosomes either mixed homogenously by sonication or not mixed. (b) Infrared absorption spectra
369 of powders containing lyophilized suspensions of CM or IM embedded within a KBr matrix.

370 Figure 3: (a) Specific absorption rate (SAR) of suspensions of chains of magnetosomes, which are able
371 (or not if embedded in a gel or deposited on a solid substrate) to rotate under the application of an
372 alternating magnetic field. (b) SAR of suspensions of individual magnetosomes, which are able (or not)
373 to rotate under the application of an alternating magnetic field.

374 Figure 4: (a) Percentage of inhibition of HeLa and MDA-MB-231 cells incubated in the presence of CM
375 and IM as a function of the magnetic field strength. (b) Mass of maghemite internalized within MDA-
376 MB-231 cells incubated in the presence of IM and CM and exposed to an alternating magnetic field of
377 frequency 198 kHz and average field strength of 20 mT during 5 to 20 minutes.

378 Figure 5: Scanning electron microscopy image of a MDA-MB-231 cell incubated in the presence of CM.
379 V designates a vesicle.

380 Figure 6: Confocal optical microscopic images of cancer cells stained with Prussian blue and incubated
381 in the absence of magnetosomes, (a), in the presence of CM, (b), and in the presence of IM, (c).

382 Figure 7: Conceptual summary describing the effect of aggregation on the penetration of magnetosomes
383 within cancer cells. The magnetosomes are either CM, (a), or IM, (b).

384

385

386

387

388

389

390

391

392

393

394

395

396

397

398

399

400

401 **REFERENCES**

- 402 1. DeNardo, S.J., DeNardo, G.L., Natarajan, A., Miers, L.A., Foreman A.R., Gruettner C., Adamson
403 G.N., Ivkov R., 2007. Thermal Dosimetry Predictive of Efficacy of ¹¹¹In-ChL6 Nanoparticle AMF-
404 Induced Thermoablative Therapy for Human Breast Cancer in Mice. *J. Nucl. Med.* 48, 437-444.
- 405 2. Kikumori, T., Kobayashi, T., Sawaki, M., Imai, T., 2009. Anti-cancer effect of hyperthermia on
406 breast cancer by magnetite nanoparticle-loaded anti-HER2 immunoliposomes. *Breast Cancer Res.*
407 *Treat.* 113, 435-441.
- 408 3. Johannsen, M., Gnevekow, U., Eckelt, L., Feussner, A., Waldöfner, N., Scholz, R., Deger, S., Wust,
409 P., Loening, S.A., Jordan, A., 2005. Clinical hyperthermia od prostate cancer using magnetic
410 nanoparticles: Presentation of a new interstitial technique. *Int. J. Hyperthermia* 21, 637-647.
- 411 4. Johannsen, M., Gnevekow, U., Thiesen, B., Taymoorian, K., Cho, C.H., Waldöfner, N., Scholz, R.,
412 Jordan, A., Loening, S.A., Wust, P., 2007. Thermotherapy of Prostate Cancer Using Magnetic
413 Nanoparticles: Feasability, Imaging, and Three-Dimensional Temperature Distribution. *European*
414 *Urology* 52, 1653-1662.
- 415 5. Kawai, N., Ito, A., Nakahara, Y., Futakuchi, M., Shirai, T., Honda, H., Kobayasi, T., Kohri, K., 2005.
416 Anticancer Effect of Hyperthermia on Prostate Cancer Mediated by Mediated by Magnetite Cationic
417 Liposomes and Immune-Response Induction in Transplanted Syngeneic Rats. *The Prostate.* 64, 373-
418 381.
- 419 6. Kawai, N., Futakuchi, M., Yoshida, T., Ito, A., Sato, S., Naiki, T., Honda, H., Shirai, T., Kohri, K.,
420 2008. Effect of Heat Therapy Using Magnetic Nanoparticles Conjugated With Cationic Liposomes
421 on Prostate Tumor in Bone. *The Prostate.* 68, 784-792.
- 422 7. Maier-Hauff, K., Ulrich, F., Nestler, D., Niehoff, H., Wust, P., Thiesen, B., Orawa, H., Brudach, V.,
423 Jordan, A., 2011. Efficacy and safety of intratumoral thermotherapy using magnetic iron-oxide

- 424 nanoparticles combined with external beam radiotherapy on patients with recurrent glioblastoma
425 multiforme. *J. Neurooncol.* 103, 317-324.
- 426 8. Zhao, Q., Wang, L., Cheng, R., Mao, L., Arnold, R.D., Howerth, E.W., Chen, Z.G., Platt, S., 2012.
427 Magnetic Nanoparticle-Based Hyperthermia for Head and Neck Cancer in Mouse Models.
428 *Theranostics.* 2, 113-121.
- 429 9. Hergt, R., Dutz, S., Müller, R., Zeisberger, M., 2006. Magnetic hyperthermia: nanoparticle
430 magnetism and material development for cancer therapy. *J. Phys.: Condens. Matter.* S2919-S2934.
- 431 10. Hergt, R., Dutz, S., 2007. Magnetic particle hyperthermia-biophysical limitations of a visionary
432 tumour therapy. *J. Magn. Magn. Mat.* 311, 187-192.
- 433 11. Hergt, R., Dutz, S., Röder, M., 2008. Effects of size distribution on hysteresis losses of magnetic
434 nanoparticles for hyperthermia. *J. Phys.: Condens. Matter.* 385214.
- 435 12. Bordelan, D.E., Cornefo, C., Grüttner, C., Wesphal, F., Deweese, T.L., Ivkov, R., 2011.
436 Magnetic nanoparticle heating efficiency reveals magneto-structural differences when characterized
437 with wide ranging and high amplitude alternative magnetic fields. *J. Appl. Phys.* 109, 124904.
- 438 13. Ivkov, R., DeNardo, S.J., Daum, W., Foreman, A.R., Goldstein, R.C., Nemkov, V.S., DeNardo
439 V., 2005. Application of High Amplitude Alternating Magnetic Fields for Heat Induction of
440 Nanoparticles Localized in Cancer. *Clin. Cancer Res.* 11, 7093s-7103s.
- 441 14. Hergt, R., Hiergeist, R., Zeisberger, M., Schüler, D., Heyen, U., Hilger, I., Kaiser, W. A., 2005.
442 Magnetic properties of bacterial magnetosomes as potential diagnostic and therapeutic tools. *J. Magn.*
443 *Magn. Matter.* 293: 80-86.
- 444 15. Timko, M., Dzarova, A., Kovac, J., Skumiel, A., Józefczak, A., Hornowski, T., Gojzewski, H.,
445 Zavisova, V., Koneracka, M., Sprincova, A., Strbak, O., Kopcansky, P., 2009. Tomasovicova N,
446 Magnetic properties and heating effect in bacterial magnetic nanoparticles. *J. Magn. Magn. Matter.*
447 321, 1521-1524.

- 448 16. Alphandéry, E., Faure, S., Chebbi, I., 2011. Treatment of cancer or tumor induced by the release
449 of heat generated by various chains of magnetosomes extracted from magnetotactic bacteria and
450 submitted to an alternative magnetic field. Int. Patent No. 061259.
- 451 17. Alphandéry, E., Carvallo, C., Menguy, N., Chebbi, I., 2011. Chains of Cobalt Doped
452 Magnetosomes Extracted from AMB-1 Magnetotactic Bacteria for Application in Alternative
453 Magnetic Field Cancer Therapy. J. Phys. Chem. C. 115, 11920-11924.
- 454 18. Alphandéry, E., Faure, S., Seksek, O., Guyot, F., Chebbi, I., 2011. Chains of Magnetosomes
455 Extracted from AMB-1 Magnetotactic Bacteria for Application in Alternative Magnetic Field Cancer
456 Therapy. ACSnano. 5, 6279-6296.
- 457 19. Mosmann, T., 1938. Rapid Colorimetric Assay for Cellular Growth and Survival: Application to
458 Proliferation and Cytotoxicity Assays. J. Immunol. Methods. 65, 55-63.
- 459 20. Yoshino, T., Hirabe, H., Takahashi, M., Kuhara, M., Takeyama, H., Matsunaga, T., 2008.
460 Magnetic Cell Separation Using Nano-Sized Bacterial Magnetic Particles With Reconstructed
461 Magnetosome Membrane. Biotechnology and Bioengineering. 101, 470-477.
- 462 21. Diem, M., Bodyston-White, S., Chiriboga, L., 1999. Infrared Spectroscopy of Cells and
463 Tissues: Shining Light onto a Novel Subject. Applied Spectroscopy. 53, 148A-161A.
- 464 22. Han, L., Li, S.Y., Yang, Y., Zhao, F.M., Huang, J., Chang, J., 2008. Research on the Structure
465 and Performance of Bacterial Magnetic Nanoparticles. J. Biomat. Appl. 22, 433-448.
- 466 23. Song, H.P., Li, X.G., Sun, J.S., Xu, S.M., Han, X., 2008. Application of a magnetotactic
467 bacterium, *Stenotrophomas* sp. to the removal of Au(III) from contaminated wastewater with a
468 magnetic separator. Chemosphere. 72, 616-621.
- 469 24. Abramson, M.B., Norton, W.T., Katzman, R., 1965. Study of Ionic Structures in Phospholipids
470 by Infrared Spectra. The Journal of Biological Chemistry. 240, 2389-2395.

- 471 25. Salazar, A., Morales, A., Marquez, M., 2011. Characterization of natural microcosms of
472 estuarine magnetotactic bacteria. *Dyna*. 72-80.
- 473 26. Draper, O., Byrne, M.E., Li, Z., Keyhani, S., Barrozo, J.C., Jensen, G., Komeili, A., 2011. Mam
474 K, A bacterial actin, forms dynamic filament in vivo that are regulated by the acidic proteins MamJ
475 and Lim J. *Mol. Microbiol.* 82, 342-354.
- 476 27. Scheffel, A., Gruska, M., Faivre, D., Linaroudis, A., Plitzko, J., Schüler, D., 2006. An acidic
477 protein aligns magnetosomes along a filamentous structure in magnetotactic bacteria. *Nature*. 440,
478 110-114.
- 479 28. Villanueva, A., Canete, M., Roca, A.G., Calero, M., Veintemillas-Verdaguer, S., Serna, C.J., Del
480 Puerto Morales, M., Miranda, R., 2009. The influence of surface functionalization on the enhanced
481 internalization of magnetic nanoparticles in cancer cells. *Nanotechnology*. 20, 115103.
- 482 29. Xie, J., Chen, K., Chen, X., 2009. Production, Modification and Bio-Applications of Magnetic
483 Nanoparticles Gestates by Magnetotactic Bacteria. *Nano. Res.* 2, 261-278.
- 484 30. Sunderland, C.J., Steiert, M., Talmadge, J.E., Derfus, A.M., Barry, S.E., 2006. Targeted
485 nanoparticles for detecting and treating cancer. *Drug Dev. Res.* 67, 70–93.
- 486 31. Wilhelm, C., Billotey, C., Roger, J., Pons, J.N., Bacri, J.C., Gazeau, F., 2003. Intracellular
487 uptake of anionic superparamagnetic nanoparticles as a function of their surface coating.
488 *Biomaterials*. 24, 1001-1011.
- 489
- 490
- 491
- 492
- 493

494

495

496

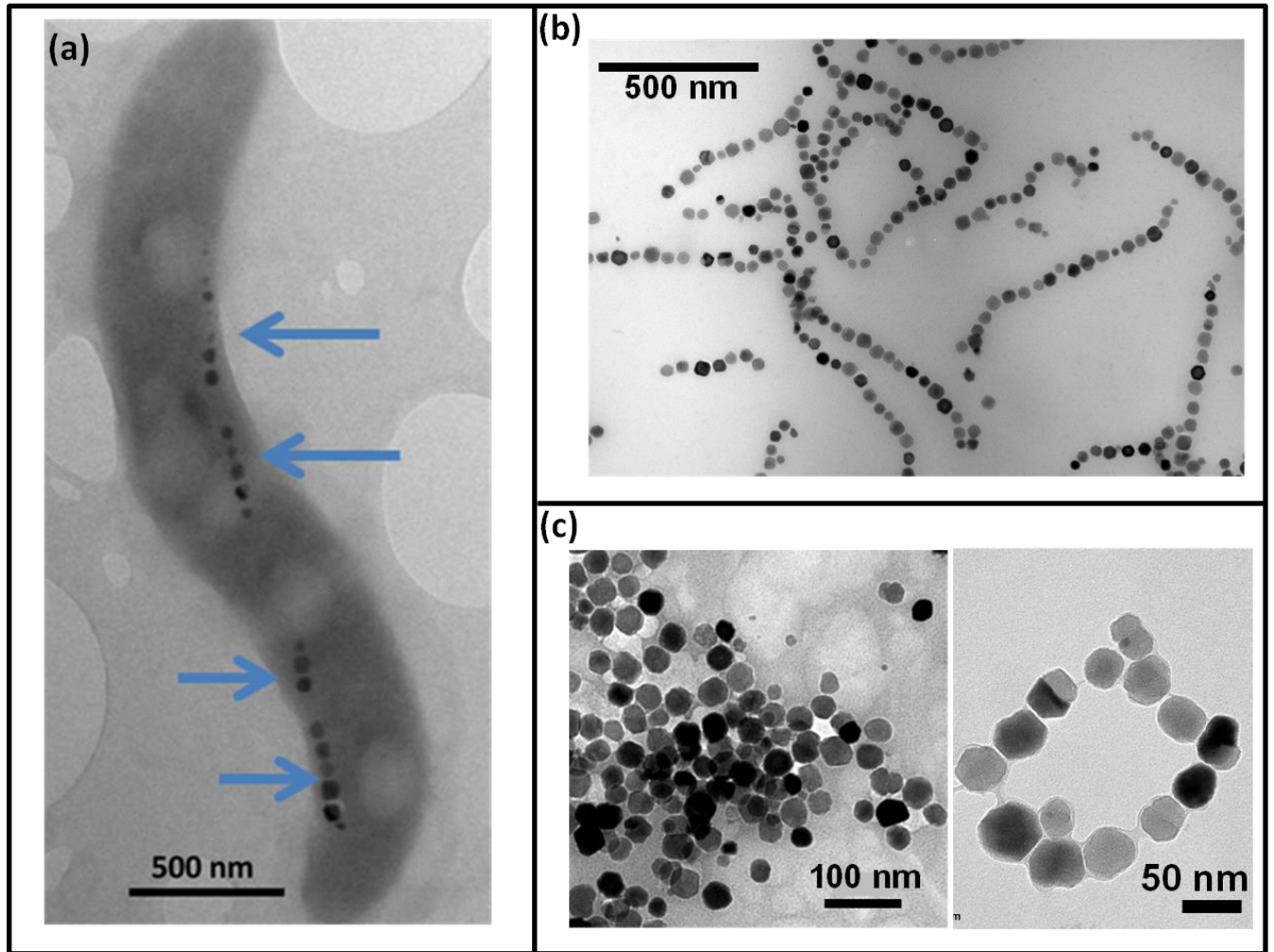


FIG. 1

497

498

499

500

501

502

503

504

505

506

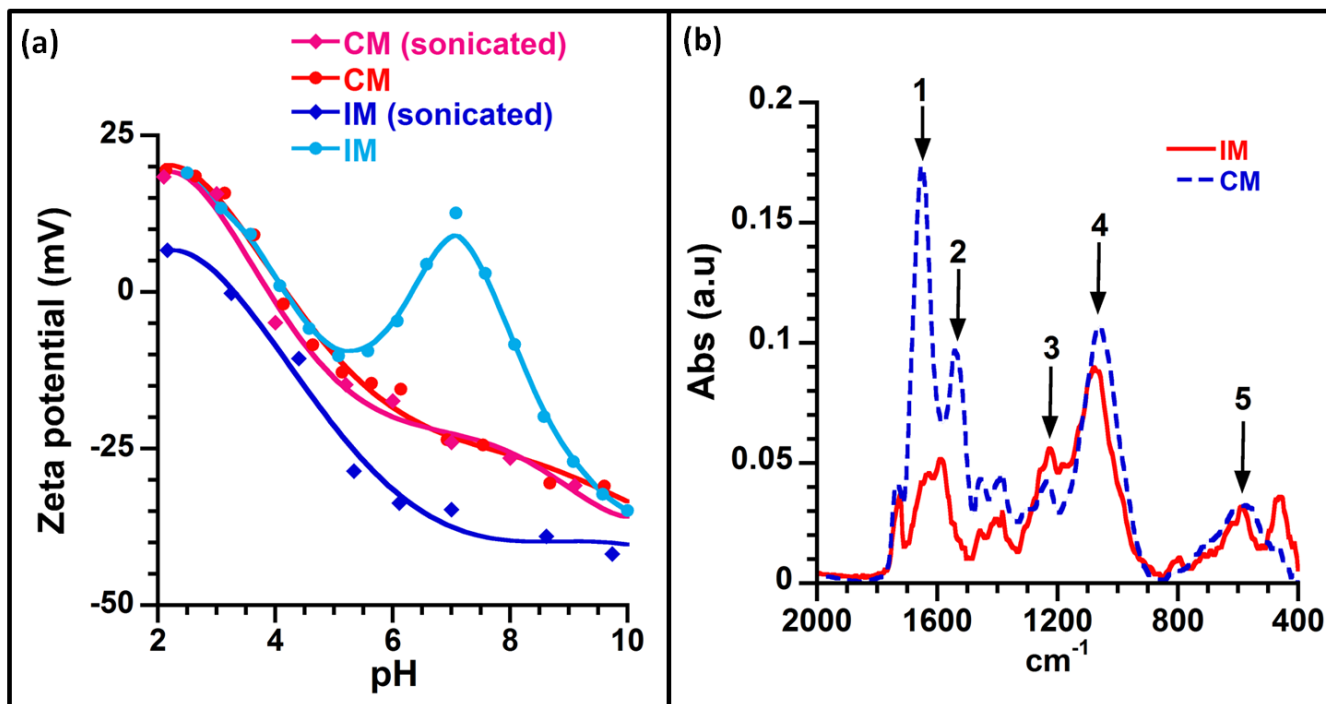


FIG. 2

507

508

509

510

511

512

513

514

515

516

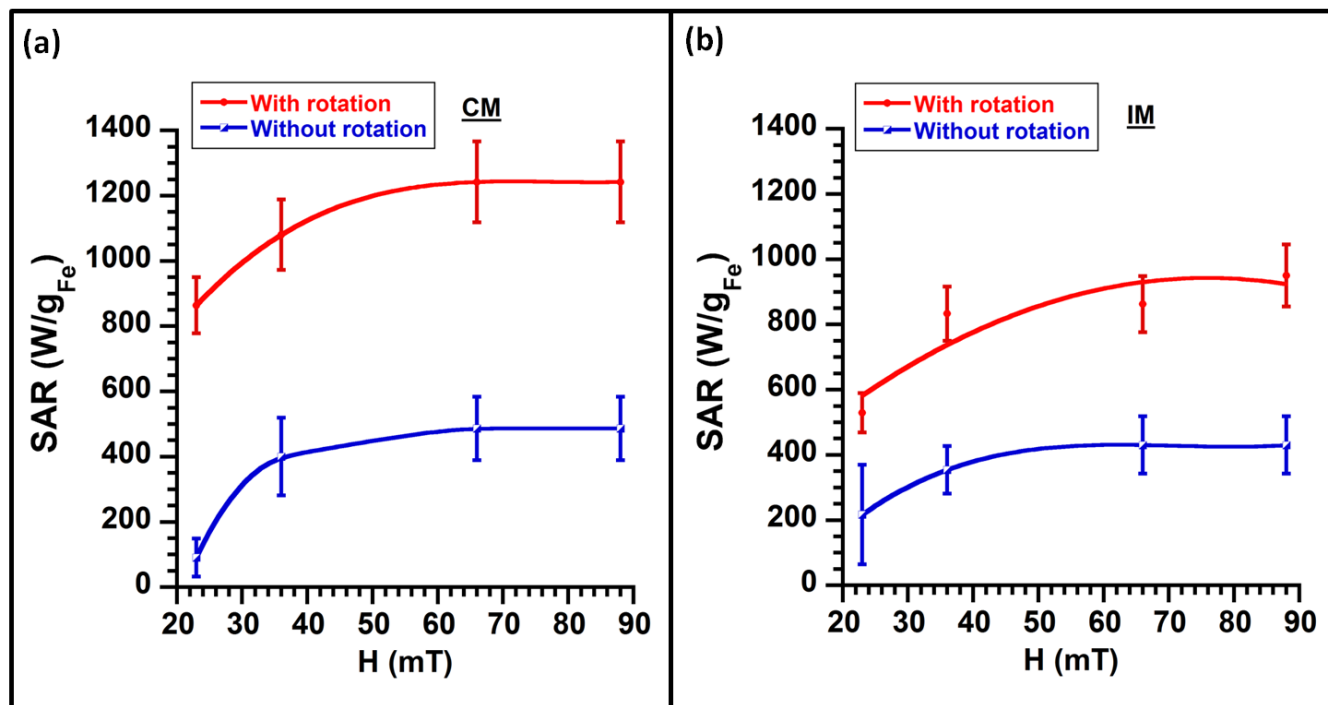


FIG. 3

517

518

519

520

521

522

523

524

525

526

527

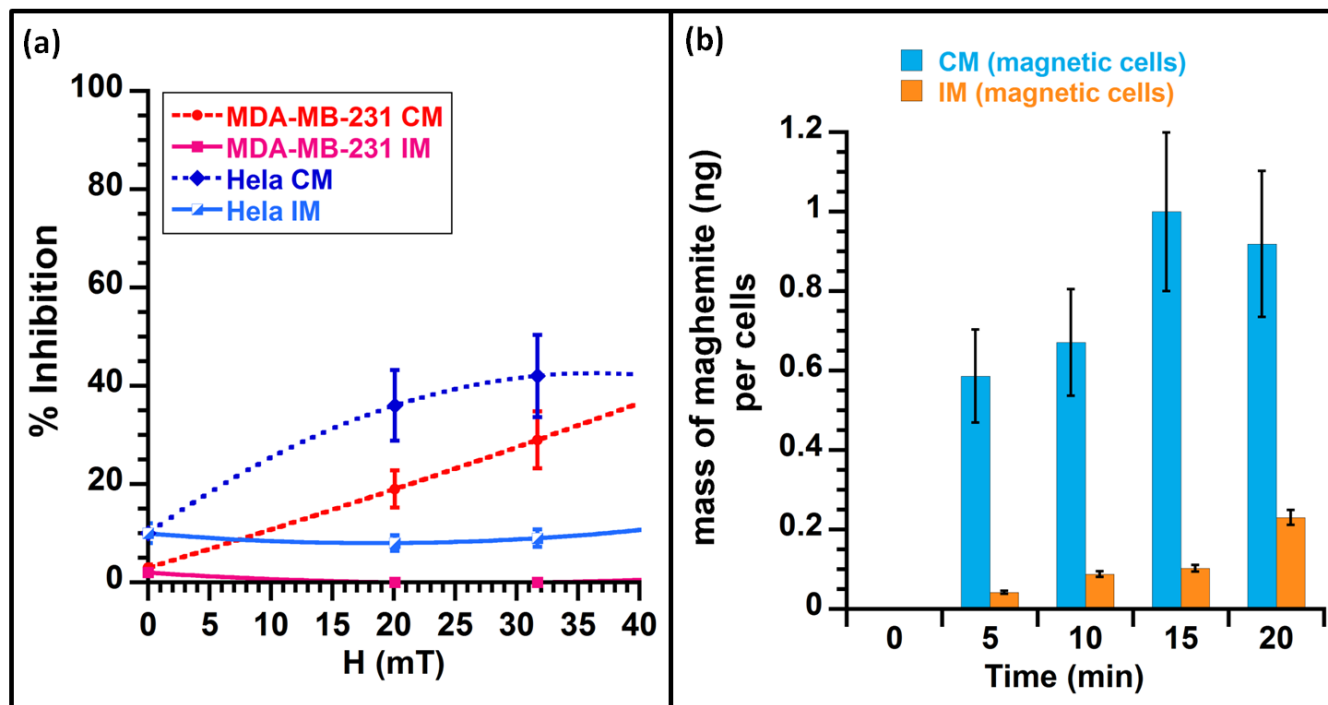


FIG. 4

528

529

530

531

532

533

534

535

536

537

538

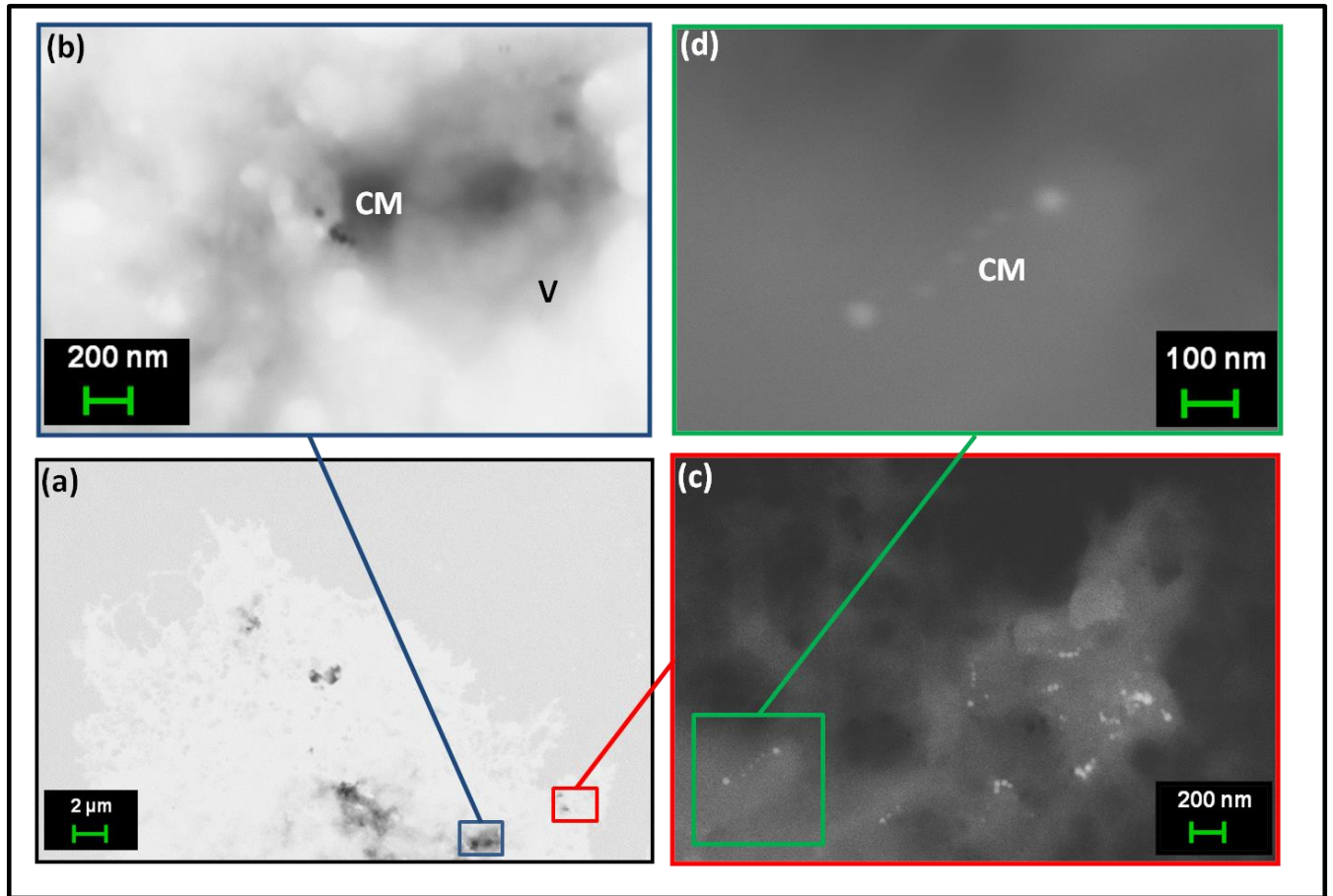


FIG. 5

539

540

541

542

543

544

545

546

547

548

549

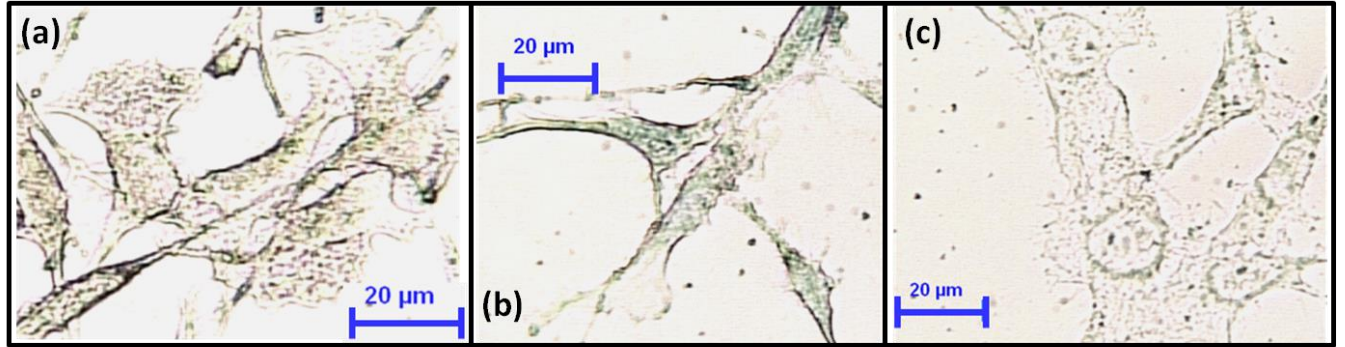


FIG. 6

550

551

552

553

554

555

556

557

558

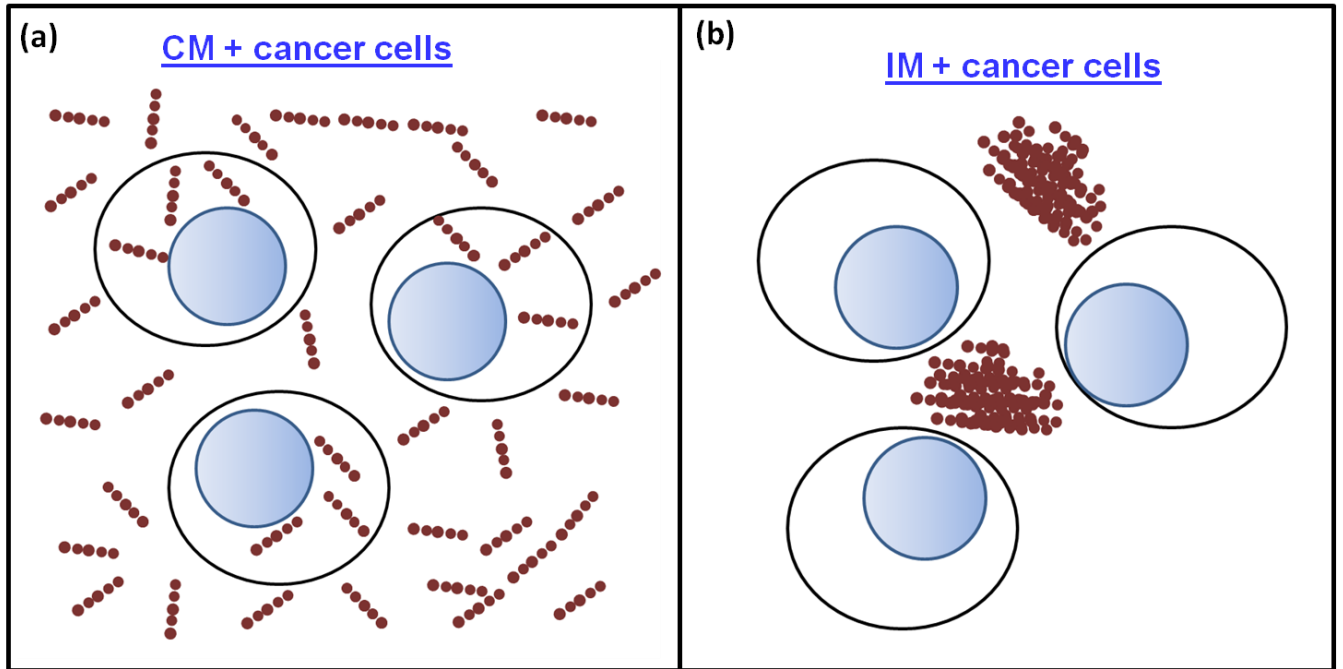
559

560

561

562

563



564

FIG. 7